A holistic system approach for short range passenger aircraft with cryogenic propulsion system

OPEN ACCESS
IOP Publishing
Superconductor Science and Technology
Supercond. Sci. Technol. **33** (2020) 044014 (14pp)
https://doi.org/10.1088/1361-6668/ab7779

A holistic system approach for short range passenger aircraft with cryogenic propulsion system

Martin Boll[1], Matthias Corduan[2], Stefan Biser[1], Mykhaylo Filipenko[1], Quoc Huang Pham[1,3], Sonja Schlachter[3], Peter Rostek[4] and Mathias Noe[3]

[1] Rolls Royce Ltd CO KG, Electrical, D-82024 Taufkirchen, Germany
[2] Siemens AG, Corporate Technology, eAircraft, D-91058 Erlangen, Germany
[3] Karlsruhe Institute of Technology- Institute of Technical Physics, D-76432 Karlsruhe, Germany
[4] Airbus Electric Aircraft Systems, D-82024 Taufkirchen, Germany

E-mail: martin.boll@rolls-royce.com

Received 1 November 2019, revised 1 February 2020
Accepted for publication 18 February 2020
Published 3 March 2020

Abstract

Currently, hybrid-electric aircraft are under investigation as one possible solution to reduce the emissions of the aviation industry according to Flightpath 2050 of the European Union. To meet the drive train's requirements on low mass while aiming for highest efficiency, superconducting technologies are regarded as a key enabling technology for drive train powers of several tens of megawatts. Within the German nationally funded project TELOS an exemplary mission profile and the physical measures of a 220-passenger aircraft are used to derive the requirements for a cryogenic-cooled serial hybrid-electric propulsion system. To optimize the total system performance, we subsequently evaluated the superconducting and cryogenic-cooled components by using computationally fast, analytical models. This approach allows quantifying the system performance by using component technologies being available today. In particular, the system performance of geared drive to direct drive propulsion units are compared and the influence of the DC bus voltage and the electric frequencies of the AC circuits on the mass and the efficiency of the drive trains are analysed.

Keywords: superconducting machines, hybrid electric drive trains, hydrogen, electric aircraft, cryogenic power electronics, systems

(Some figures may appear in colour only in the online journal)

1. Introduction

The number of passengers travelling by aircraft is constantly rising with an annual rate of about four percent. Due to this development, the effect of the improving fuel efficiency of aircraft and their engines is overwhelmed which leads to increasing absolute emissions of the overall civil aviation sector [1]. This issue is in stark contrast to the goal of reducing the absolute CO_2 emissions of the aviation sector by 50% until 2050 [2]. Therefore, disruptive technological approaches as hybrid-electric propulsion systems for aircraft are required to achieve this ambitious goal [1, 3, 4].

The largest share of aircraft is operating within the short and mid-range distance, covering distances about 1000–3000 nautical miles (nm) and up to 240 passengers (PAX) [5]. However, to create an advantage by applying hybrid-electric propulsion systems to such aircraft requires low masses and high efficiencies of the electric components [6] that are very challenging compared to the state of the art [7]. The use of superconducting and cryogenic-cooled components could potentially overcome these limitations. Firstly, due to the

enormous current carrying capabilities of superconductors, using them in electric machines or cables can reduce the masses and required voltage levels of such components. Secondly, when cooling these components with liquid hydrogen, the evaporated hydrogen can be used further as a fuel for power generation [3, 6] instead of requiring energy densities for batteries that are orders of magnitude higher [8] than the state of the art [7]. Power- and thrust generation of aircraft by combustion of (liquid-) hydrogen instead of kerosene have been part of numerous investigations during the past [9]. Investigations showed that using hydrogen reduces the CO_2 -emissions while increasing the efficiency of the engine [10]. However, due to its low volumetric density, the volume to store the required amount of liquid hydrogen in the aircraft removes this advantage on an aircraft-level [11]. It should be noted, that the Soviet aircraft TU-155 successfully passed experimental flights between Moscow and Kiev with hydrogen powered engines in 1988.

Here, an approach to determine the mass and the efficiency of a cryogenic electric propulsion systems (CEPS) in dependency of internal component parameters as the electric frequency or the DC link voltage is presented. Using analytical models of the electric components that cover the domains of electromagnetics, thermics and mechanics and their interactions, not only their masses and efficiencies but also their cooling requirements are extracted. To account for the mass of the cooling system, an analytical model to compute the mass of a tank system to store liquid hydrogen is used.

The approach is showcased for a hypothetically hybrid-electric 220 PAX aircraft with a mission range of 2500 nm. We assume the power generation to be fueled with a mixture of kerosene and hydrogen gas that evaporated during the cooling of the CEPS with liquid hydrogen. The dependency of mass and efficiency of the CEPS and its constituting components are investigated for varying voltage levels on the DC bus, the mechanic rotation speed of the superconducting machines and the electric frequencies in the AC parts of the system.

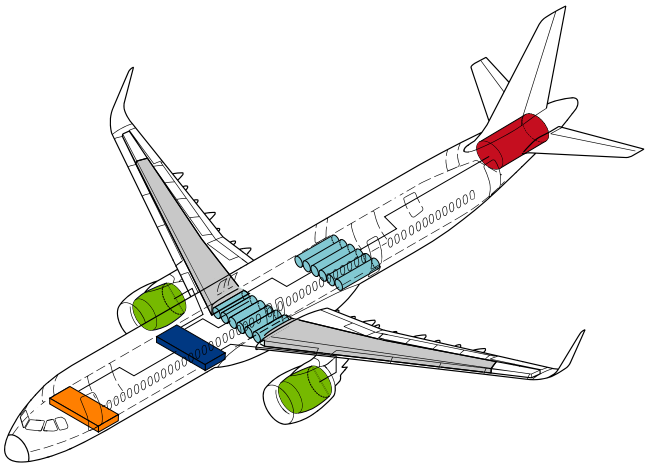

(a) Re-equiped reference aircraft

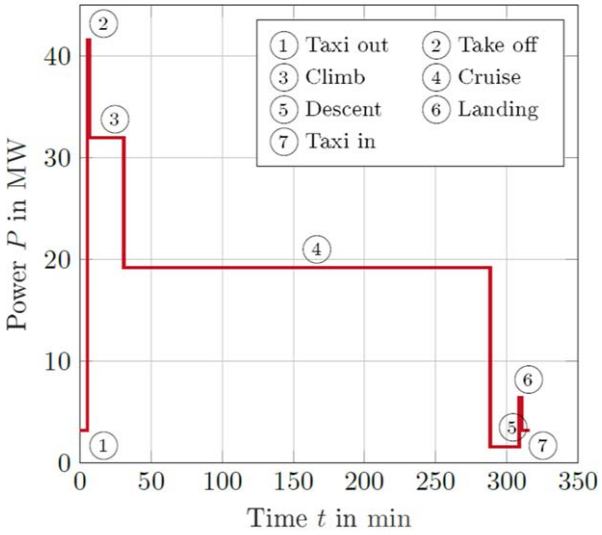

(b) Mission profile

Figure 1. Schematic illustration of the hybrid-electric re-equipped aircraft. (a) The electric propulsion units (green) are placed at the position of the turbofan engines underneath the wing of the aircraft. The required power is generated by the AC generation units (red) at the back of the fuselage. The EPU and the generation are connected via HTS cables at the power distribution center (blue). The kerosene tanks in the wings remain unchanged, whereas the cylindrically-shaped tanks (Center tank and auxiliary center tanks (ACT)) in the fuselage contain liquid hydrogen. (b) Typical power demand during different phases of a mission with a cruise phase of 2500 nm. The largest power of about 41 MW is addressed only during the phase of take-off. During the cruise phase, less than half of the installed power is required to propulse the aircraft.

2. Showcase and modelling approach

2.1. Re-equipped reference aircraft

The propulsion system of the hybrid-electric aircraft is a fully turboelectric approach. A general scheme that illustrates the relative dimensions of the reference aircraft and the positioning of the electric components is shown in figure 1(a). The original aircraft has an overall length of 44.5 m and a maximum take-off weight of 101 tons. The two electric propulsion units that drive the fans which provide thrust to the aircraft remain at the same position as the propulsion units in the original aircraft. They are connected with two HTS DC power lines each to the power distribution center. The generation units that are placed at the back end of the aircraft fuselage provide the largest share of the aircraft's electric power. The generation units are also connected with HTS DC power lines to the power distribution center. Optionally, a battery unit can be placed in the front of the aircraft fuselage, not being considered in this study. The liquid hydrogen tanks are placed at the position of the center tanks in the fuselage of original aircraft. The kerosene tanks in the wings of the original aircraft remain untouched. All positions, distances, and measures are referenced to the operation manual of the commercially operated A321neo XLR [12].

2.2. Architecture

The basic architecture of the hybrid-electric drive train is shown in figure 2. The required thrust is delivered by two

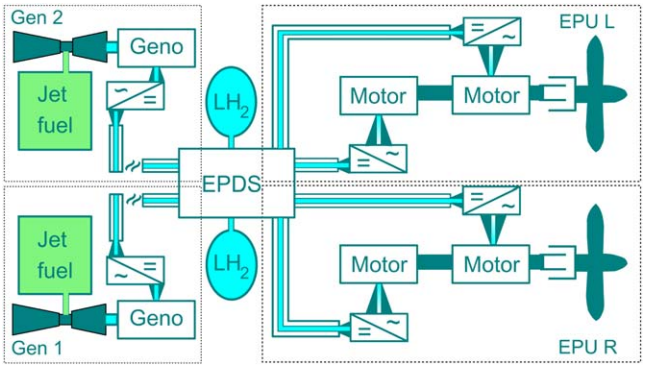

Figure 2. Cryogenic electric propulsion system (CEPS): All electric components are cooled with liquid hydrogen which is provided by tanks in the fuselage of the aircraft. Two power generation units drive two electric propulsion units. Each propulsion unit contains two machines, whereas one is powered by one power generation unit and the other machine by the second, which enhances the reliability of the system. The generation units are mainly fueled with kerosene but are also able to burn hydrogen after it has been used to cool the components of the electric drive train.

electric propulsion units (EPU L and EPU R). Each EPU contains a fan that is driven by two axially stacked superconducting machines that share the same shaft. The machines are driven by individual inverter units that are operated in the cryogenic temperature range. These units convert the DC power that is provided by superconducting DC transmission lines into AC current feeding the machines. Optionally, gearboxes that transmit the mechanical rotation speed of the machines to the fans can be included. The use of a gearbox allows optimizing the fan and the superconducting machine independently, i.e. reaching high circumferential speeds by increasing the mechanical rotation speed of the machine while keeping the allowed installation space. In this study, only the characteristics of the machines are varied whereas the fan remains constant, assumed to meet the specifications of the fan of reference aircraft with a diameter of $d_{fan} = 2.06$ m and a maximal rotation speed of $n_{fan} = 3500\ \mathrm{min}^{-1}$ [13].

Both EPUs are connected to the electric power distribution center that is placed at the position where the wings are connected to the fuselage. Here, the four power transmission lines of the EPUs are fed with the electric power of the two power generation units GEN 1 and GEN 2. To facilitate balancing of the thrust in case of a power generation unit failure, one generation unit powers one machine of the EPU R and another of the EPU L respectively. Both power generation units are placed at the back of the fuselage containing two superconducting generators that are driven by turboshaft engines. These engines are assumed to be fueled by kerosene and the hydrogen that has been used as a cooling medium of the electric components before. It has been shown that the efficiency of the combustion process of kerosene can be optimised by adding 10%–20% of hydrogen without any significant degradation when increasing the ratio even further [14]. The storage tanks for liquid hydrogen LH_2 are placed in the positions of the fuselage tanks of the reference aircraft [12]. The amount of hydrogen that boils off the tank during the operation of the aircraft can be added to the combustion cycle.

Table 1. Requirements and global variables to the subsystem design of the EPU, the generation unit and the liquid hydrogen tank. Besides the voltage level, the ambient conditions at a flightlevel (FL) of up to 40 000 ft is considered. The maximum diameter $d_{EM,\max}$ are linked to the actual design of the fan, which tend to require a large ratio of fan diameter to machine diameter. The volume limits to place the hydrogen tanks are derived from the respective kerosene tanks in the original aircraft. The maximum accessible height $h_{\max}$ and width $w_{\max}$ are deduced from the cross section of the fuselage [12].

Type	Symbol	Unit	Range/Value
Global	V_{DC}	V	1000–4000
	T_a	K	218–318
	$p_{a,\max}$	mbar	1013
	FL	ft	40 000
EPU	$f_{el,EPU}$	Hz	175–1000
	P_{EM}	MW	10.5
	n_{EM}	min^{-1}	3500–15000
	$d_{EM,\max}$	m	0.6
	$l_{EM,\max}$	m	0.9
	$l_{Cable,EPU}$	m	8.0
Gen	$f_{el,gen}$	Hz	333–1000
	P_{Gen}	MW	21.0
	n_{Gen}	min^{-1}	10 000
	$d_{Gen,\max}$	m	0.5
	$l_{Gen,\max}$	m	2.0
	$l_{Cable,gen}$	m	18.0
Tank Center	$l_{\max}$	m	2.55
	$h_{\max}$	m	1.24
	$w_{\max}$	m	2.7
	K	—	9.0
Tank ACT	$l_{\max}$	m	1.85
	$h_{\max}$	m	1.24
	$w_{\max}$	m	2.7
	K	—	9.0

2.3. Requirements

An excerpt of varied global parameters and fixed system requirements are shown in table 1. The maximum flight level (FL), the operational ambient temperature range T_a and the maximum ambient pressure $p_{a,\max}$ are acquired from the European certification specifications document for large aircraft (CS 25) [15]. The same applies to the safety factor $K = 9$ on hydrostatic design conditions of fuel tanks that are placed within the fuselage (CS 25.963). The factor is considered during the design of the liquid hydrogen storage tanks. The power requirements of the electric propulsion and the generation units are deduced from the power requirements during take-off 1(b) and the architecture of the propulsion chain 2. Using the latter, the lengths of the superconducting power distribution cables $l_{cable,EPU/Gen}$ are derived. Furthermore, it is

assumed that the diameter $d_{\max,EM}$ and length $l_{\max,EM}$ of a superconducting machine in the electric propulsion unit does not exceed the measures of the core engine in the turbofan [13] that powers the reference aircraft [12]. The range of investigated mechanical rotation speeds is caused by different reasons. First, for even higher mechanical rotation speeds at the same radii, the rotor retention with a sleeve can not be achieved, forcing the diameter of the rotor radius to shrink. However, the size of a pole in such a small rotor requires superconducting coils that feature bending radii of the HTS tape and the MgB_2 wire which are mechanically not feasible [16]. The same reasoning applies for the investigated range of the number of pole pairs. Furthermore, the AC losses which are caused by high electric frequencies can only be removed up to a certain value set by the cooling process, limiting the range of pole pairs even further. All measures of the generation unit are deduced from the size of the aircraft fuselage [12] and the characteristics of state of the art turboshaft engines [17].

3. Modelling

Firstly, this study aims to identify the influence of a gearbox in between a fully superconducting machine and the fan on the overall key performance indicators (KPIs) of the drive train. Since the mechanical rotation speed directly influences the electric frequency in the system, component models which include frequency-dependent loss models are used, see sections 3.1 and 3.3. By using an analytical model that determines the mass of a tank that stores the required amount of liquid hydrogen (section 3.5) to cool these components during the mission of the aircraft, a penalty mass that prices finite efficiencies is computed. Secondly, the dependency of the overall system KPIs on the DC voltage level V_{DC} of the HTS transmission line is evaluated. Since changing the voltage level directly affects the transmitted current, the voltage dependence of current leads and the transmission line (section 4.4) is obvious. However, many studies on the system level neglect the consequences a particular voltage level can bring up for the electric machine and the power electronics. In case of a direct liquid cooled superconducting stator winding, an increased required electric insulation thickness due to higher voltage levels increases the thermal resistance thus impeding heat dissipation of the occurring AC losses. Here, the layout of the machine insulation systems is done at 4000 V and overshoot factors one expects by using pulse-width modulated power electronics. In the case of the power electronics, the voltage level will change the active and passive modules that can be used which directly affects the mass and the efficiency of a possible inverter.

The parameters which are exchanged between the component models to compose an EPU subsystem are shown in figure 3. For each unique set of requirements and global variables **x** the KPIs of the subsystem are computed. The requirements of power and rotation speed of an initial machine design need to fulfill the conditions during the take-off of the aircraft. For each of these designed unique subsystems, the performance in all phases of the aircraft's

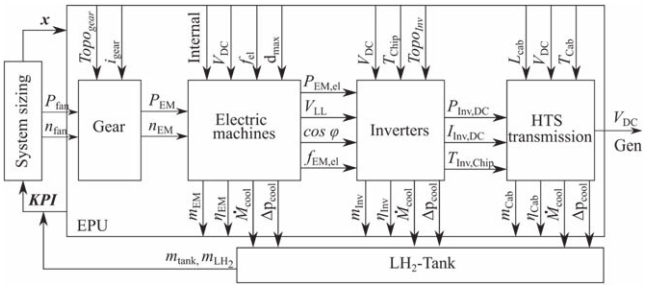

Figure 3. Modeling of EPU subsystem: For a unique set of requirements and global variables **x** the subsystem is sized at the power requirements during take-off of the aircraft. In this study, variables are the voltage level V_{DC} and the electric frequency f_{el} which is discretized to $f_{el,EM}$ by the mechanical rotation speed of the electric machine n_{EM} and its possible numbers of pole pairs. Requirements include all restrictions due to limited installation space and information about the ambient conditions at the different flight levels. For all components, the main KPIs as mass, efficiency and required cooling are computed. For each unique set of designed components, the efficiencies and cooling requirements are computed at every point of the aircraft mission. The resulting required amount of hydrogen for a mission of the aircraft is used as an input parameter to the tank model.

mission (see figure 1(b)) is calculated to determine the required amount of liquid hydrogen during a full mission.

As the propulsion system that is depicted in figure 2 is extensive and complex, showing the dependencies of the whole system on global variation parameters as the voltage level would be overwhelming and disguise their origin on the component level. Therefore, the models of the electric components and the hydrogen tank are presented in the following section. The basic modeling approach and assumptions are explained.

3.1. Fully SC machines

The electric machines for propulsion and generation are assumed to be fully superconducting radial synchronous machines. A radial cut through the machine architecture is shown in figure 4. The coils in the rotor are DC racetrack coils wound with state of the art 2G HTS tapes, operated at engineering current densities up to 300 Amm^{-2}, a value which has been achieved experimentally [16]. In contrast, the AC stator coils are assumed to consist of 114 multifilament MgB_2 wire by HyperTec [18]. Both, the windings of the stator and the rotor, are cooled with liquid hydrogen to operational temperatures between 20 and 25 K. The yoke is placed outside the cryogenic area to avoid the occurring losses in the iron being dumped in the cryogenic cooling liquid.

An analytical model was developed that determines the main KPIs of the machines for the given global requirements. The approach considers electromagnetic, thermal, mechanical, and insulation aspects of the pre-designed machines. Moreover, the interdependencies between these disciplines are taken into account. Starting with initial assumptions, machine geometry and architecture are proposed for which the magnetic field distribution is computed. Using this distribution and the frequency f_{el} of the field, a coupled electric

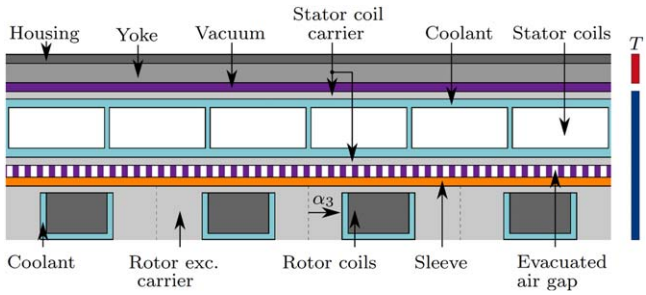

Figure 4. Architecture of fully SC machine: Basic machine architecture assumed in the analytical modelling process. The color scale on the right side indicates the cryogenic and the non cryogenic area of the machine. α_3 represents the opening angle between two adjacent coils of the rotor, one of the internal optimisation parameters of the machine model [19].

and thermal modeling is used iteratively to deduce the engineering current density J_e at the working point of the stator coil. The value of J_e is set such that the highest local loss density p_v can still be cooled. The total losses in the stator P_v and its cooling requirements $\dot{M}_{co}$ are computed integration of the local loss density along the field and current density distribution of the machine. The length of the machine l_{eff} is scaled to meet the targeted torque T. After adapting the machine length, the required thickness of the retention sleeve and the cryowalls are computed again to verify the size of the magnetic airgap. If this criterion is not met, the machine model is iterated. A detailed description of the machine model and the involved materials is given in [19].

This allows to work out the sensitivities of the machine KPIs with respect to the varied external parameters of the propulsion system. For example, the variation of the mechanical rotation speed of the machine n_{shaft} has direct consequences on mechanics, electromagnetics and thermics. The thickness of the rotor sleeve is scaled such that it retains the rotor against the mechanical loads by the rotating masses. Therefore, its required thickness increases for larger rotation speeds of the machine which leads to bigger magnetic airgaps. Consequently, the amplitude of the magnetic field at the stator coils is lowered which changes the AC loss density in the stator coils. Since the electromagnetic loss and the liquid cooling mechanism are treated in a coupled model [19], the cooling requirements of the machine are directly affected.

The computed machine mass includes the masses of active and passive parts of the machine, such as the coil carrier in the rotor and the stator, the rotor retention sleeve, a machine housing, axial machine covers, and a rotor shaft. The losses of the machine include the AC losses of the stator coil and the iron losses of the yoke.

3.2. Gearbox

To compare the mass and the efficiency of the direct drive to the geared drive solutions of the EPUs, the gearbox that is installed in between the superconducting machines and the fan. The mass and efficiency of these gearboxes were computed with an analytical tool that controls the commercially available software KissSoft [20] via an interface. The sizing and computation of the gear is done according to the ISO norm ISO 6336:2006 B. For a given lubrication oil at an inlet temperature of 70 °C the gear is designed such that the maximum temperature of the oil at 110 °C is not exceeded due to the different load- and no-load dependent loss channels [21]. Depending on the required power, the rotation speed of the fan and the machine, gears, shafts, bearings and housing are designed for two different gear topologies, spur and planetary gearboxes. In this study, planetary gears were selected due to their lower mass and higher efficiencies for the requirements of table 1. With dry masses of about $m_{gear} =$ 200 kg and maximum efficiencies up to $\eta_{gear} = 0.996$ the gearbox characteristics are in the same range as state of the art gearbox in a geared turbofan [13]. The required amount of lubrication oil is computed via empirical polynomial correlation functions that relate the loss with the required amount of oil for forced lubrication cooling. The required mass flow of oil can be used as an input parameter to scale the size of a heat exchanger that is capable to transfer the heat input of the gearbox to the accessible airflow in the propulsion unit.

3.3. Cryogenic power electronics

The choice to operate the power electronics at cryogenic temperatures is based on two reasons. Firstly, if the power electronics would be used at usual temperatures of about 370 K, huge leads that feed the current from the warm to the cryogenic parts are required. To avoid these additional masses, ideally, the power electronics should operate at the same temperature as the superconducting machines and the HTS power cables. Secondly, it has been shown that lowering the operating temperature affects also the performance of the devices themselves [22].

Multiple studies have measured and modeled the cryogenic performance of active devices such as IGBTs and MOSFETs [23]. Si-IGBTs show reduced switching and transconductance losses at 77 K by about 60% and 24% respectively when comparing to room temperature [22]. However, for even smaller temperatures the carriers freeze out which leads to a rapid increase of the on-state resistance below temperatures of about 50 K. For silicon, the carrier concentration is a few ten orders of magnitude smaller at 25 K compared to 100 K [24]. Therefore, we limit the lowest the operating chip temperature to 100 K.

DC/AC inverters can be realized in different topologies, differing in the height of the single-step output voltage and the total harmonic distortion (THD). Our model considers two-level (2L-), three-level neutral point clamped (3LNCP-) and five-level stacked multicell (5LSMC-) DC/AC voltage source inverters. Most parts of our design process are based on the extensive work in [25]. First, the voltage configuration of switches and diodes for the given operation point is determined. To do this, a database with semiconductor modules and their properties at cryogenic temperatures is set up. In this study, we focus on the cryogenically tested Si-IGBT 1700 V module by Infineon [26]. A scalable semiconductor characteristic is established from the data which is then used to perform a coupled calculation of electric and

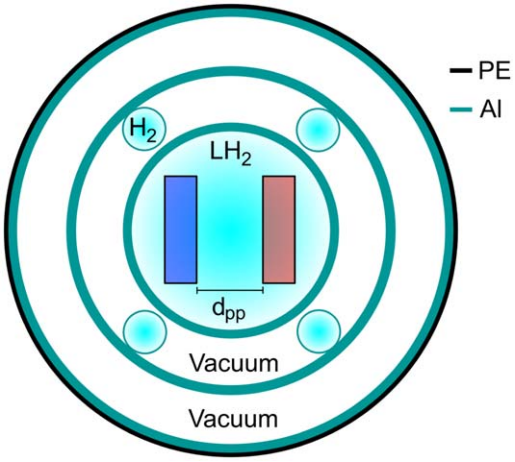

Figure 5. Schematic view on the HTS cable: The two poles of stacked HTS conductors are placed in the inner shell (red and dark blue rectangles) of the cryostat. The stacks are circumvented by flowing LH_2. The next outer shell is evacuated and contains four pipes that allow evaporated hydrogen flowing backward. The outer shell of the cryostat is again evacuated and surrounded by the outermost cryostat wall and a polyurethane layer for mechanical protection. All cryostat shells are assumed to be made of an aluminum alloy that is resistant to hydrogen.

thermal performance. The maximum bias voltage is limited to 50% of the rated blocking voltage to retain low failure rates in presence of cosmic radiation effects at the flight level of 40 000 ft [27]. Based on the operation point the losses of the semiconductor modules are calculated. The semiconductor modules, as well as the heat sink, i.e. an aluminium cooling plate, is sized such that the chip temperature increase due to the losses at the calculated operating point is below a certain limit and that the waste heat can be removed via the cooling plate. The cooling plate carries the flow of liquid hydrogen. Furthermore, the DC link capacity is calculated based on the expected current ripple calculated analytically based on using a method provided in [25]. Again, a database of commercially available pps metallic film capacitors that were tested at cryogenic temperatures is used [28]. The sizing process also includes a mass estimation of the gate driver units and a simple aluminium housing.

For each topology we computed inverters in the range of V_{DC} and $f_{el,EM}$ according to table 1. The switching frequency is kept constant ten times the electric output frequency $f_{el,EM}$. The operation temperature of the chip is assumed to be 100 K while keeping the temperature of the cooling liquid in the cooling plate is 22 K.

3.4. HTS DC transmission

The model of the cable and its cryostat is based on the work of Schlachter *et al* [29] which had an HTS DC transmission system for 10 MVA at 3 kV as target values. A scheme of the basic architecture is shown in figure 5. Taken this architecture, a model was developed which scales the dimensions of the components for the respective global requirements.

The measures of the inner shell of the cryostat are determined by criteria set by the current and the DC voltage level of the cable. Firstly, the required number of tapes per stack to conduct the current is determined, taking into account the reduced current capability due to the magnetic field of neighboring tapes. As the conductor, a commercially available HTS tape by Theva was assumed [30]. Secondly, the distances between the two poles and from one pole to the cryowall are determined. The Lorentz forces which act between the two poles need to be smaller than the maximum force the support structure of each pole can withstand. Using this, a minimum required distance between the poles $d_{pp,F}$ is calculated. Furthermore, for the respective voltage level and an estimated overshooting voltage due to the PWM inverter, the minimum required distances between the two poles $d_{pp,V}$ and between the cryowall and the poles $d_{wp,V}$ to avoid arcing are computed. The inner diameter d_{in} of the core cryostat is set a combination of these distances and adding the thickness d_{stack} of the poles:

$$d_{in} = 2 \cdot (d_{stack} + d_{wp,V}) + \max(d_{pp,F}, d_{pp,V}). \quad (1)$$

For each resulting cross-section including the two HTS stacks, the pressure drop of liquid hydrogen is computed with an analytical model of a mixed-phase flow [31]. The required mass flow of liquid hydrogen is adapted according to the losses in the transmission line. The overall loss contains the AC loss in the HTS stacks caused by AC current ripples [32], thermal loss of the cryostat, losses at the coupling between the current lead and the HTS stacks, and the losses of the current lead itself. Overall, we found the loss of the copper current leads from 100 to 20 K being dominant, lying in the range of about 20–350 W depending on the transmitted power and the voltage level. The thickness of the cryowalls is scaled to avoid buckling due to differential pressure at the different sides of the respective walls. The mechanical and thermal material parameters of the high-strength and hydrogen resistant aluminium alloy that is used for the cryowalls has been determined experimentally [16].

The total mass of the HTS transmission line is computed as the sum of all its constituents. The masses of the superconductors m_{HTS}, its required support and insulation structure m_{supp}, the (cryo-)walls m_{wall}, the current leads m_{lead}, and the coupling between the leads and the HTS stacks m_{couple} are taken into account:

$$m_{trans} = m_{HTS} + m_{supp} + m_{wall} + m_{lead} + m_{couple} \quad (2)$$

3.5. LH2 tank

To determine the influence of finite efficiencies during the operation of the cryogenic components, a model that determines the mass of a tank to store the required amount of liquid hydrogen was developed. The model is similar to approaches that can be found in the literature [33, 34]. The geometric, mechanical and thermal architecture of the tank is designed while respecting ambient atmospheric conditions and restrictions of the installation space linked to the aircraft. The iterative modeling approach and a description of

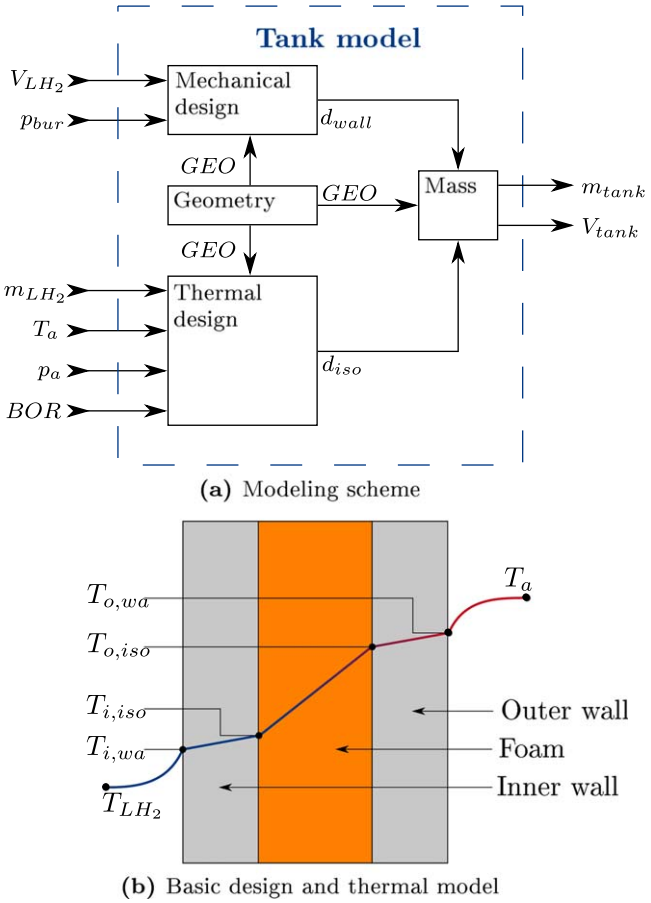

Figure 6. LH_2-tank modelling approach (a): The geometry of the inner tank is scaled according to the required volume V_{LH_2}. Its structure is mechanically designed such that it can withstand the required storage pressure which is linked to the pressure drops in the cryogenically cooled electric components and gyrometric loads. Since the maximum required pressure including the summarised pressure drop in the components is about 1.6 bar, the operational pressure is set this value. Therefore, the resulting storage temperature of hydrogen is slightly above 21 K at the saturation point. Moreover the thermal design shown in (b) needs to be fulfilled to achieve the target boil-off-rate *BOR*. The thermal model takes into account heat transfer by conduction in the structure of the tank and convection between the two phase hydrogen mixture and the inner aluminium wall of the tank.

the thermal model are illustrated in figures 6(a) and (b), respectively.

The masses of instrumentation, valves and filling sensors are considered by an estimation function that was obtained by interpolation of these supplementary masses of different sized liquid hydrogen tank designs for aviation applications [9, 35, 36]. We assume the inner and outer tank walls to be fabricated by a high strength hydrogen resistant aluminium alloy that divided by a polyurethane isolation layer [9]. The geometrical shape of the tank is limited to cylinders with half-dome end caps. Given the geometrical constraints of table 1 two hydrogen tanks per accessible volume are assumed. The separated storage tanks and their respective transfer lines to the EPDS increase the reliability of the cooling and therefore also the propulsion system.

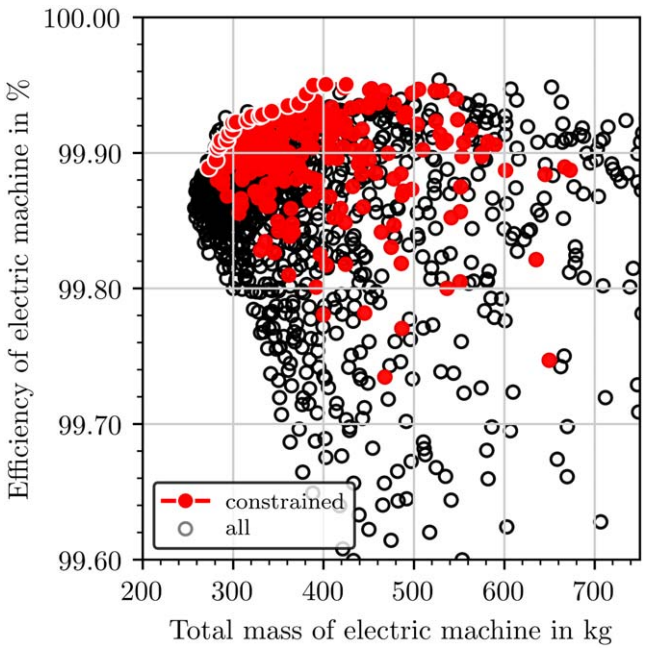

Figure 7. Fully superconducting machine: Mass and efficiency of 10.5 MW direct drive $n = 3500\ \mathrm{min}^{-1}$. The black circles show all possible machine configurations without taking into account the constraints which are set by the installation space. In contrast, the red data points take into account the limits in machine diameter and machine length. The red dots with white-colored edge represent the pareto-optimal curve that shows the limit of achievable efficiency for the respective machine mass.

4. Results

4.1. Superconducting machines

Fully superconducting machines that fulfill the global requirements of the electric propulsion- and generation- units which are shown in table 1, were modeled. In this subsection, the discussion will be focused on the machines of the electric propulsion unit. For each unique set of requirements regarding the mechanical rotation speed $n_{SC,EM}$, the DC link voltage V_{DC}, and the electric frequency $f_{el,EM}$, superconducting machines are modeled. As described in [19], a huge set of internal machine parameters are varied to optimize the performance of the machines. The influence of the mechanical rotation speed and the restrictions in diameter and length on the achievable masses and efficiencies are of particular interest. All machines are designed to resist 20% extra of their targeted mechanical rotation speed n_{EM}. In figure 7 the total mass and the efficiency of fully superconducting machines with a power of $P = 10.5$ MW directly driving the propulsion fan with a rotation speed of $n_{EM} = 3500\ \mathrm{min}^{-1}$ are shown. The influence of the constrained installation space on the minimum achievable machine mass can be observed. The maximum power to weight ratio (ptw) reaches about $38.1\ \mathrm{kW\ kg}^{-1}$ whereas $40.4\ \mathrm{kW\ kg}^{-1}$ could be achieved hypothetically without taking into account restrictions of the installation space listed in table 1. The red-faced and white circled data points show the pareto-optimal machines,

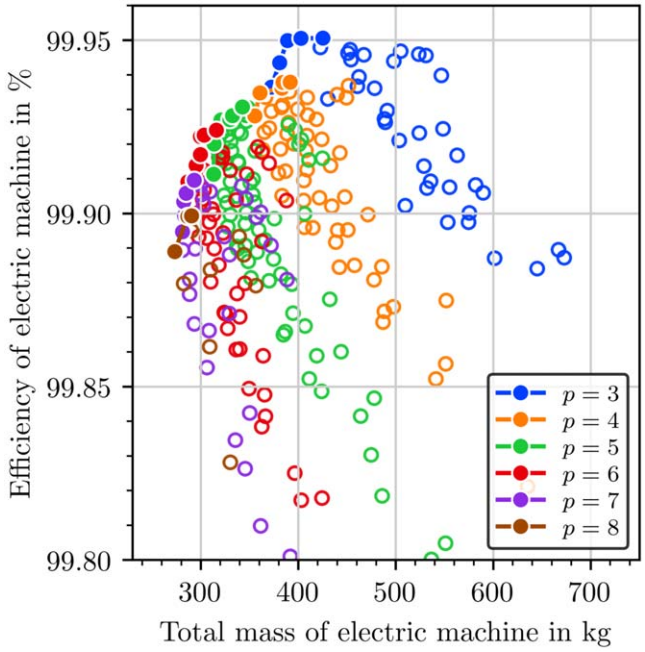

Figure 8. Stator Losses versus electric frequency: For each number of pole pairs the three machines with about the same working flux density in the stator $B_{s,wp}$ are pre-selected. The losses increase almost linear with frequency as it is expected at fields amplitudes which fully penetrate the superconducting wire.

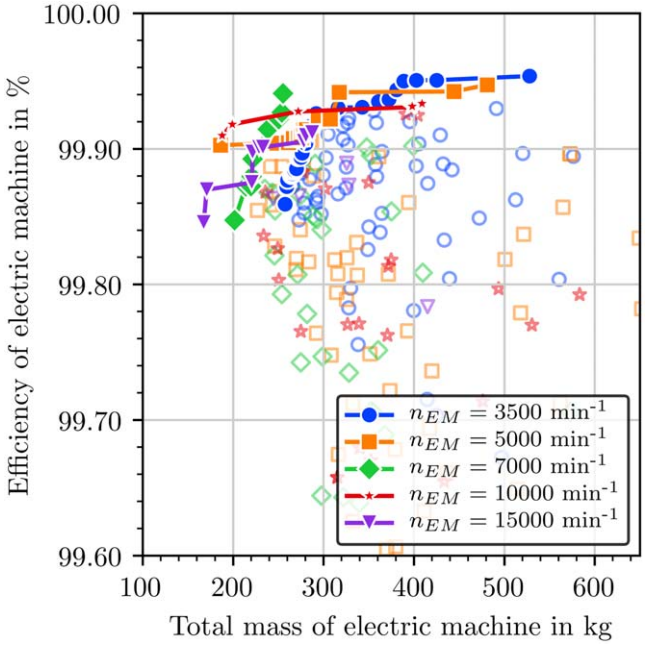

Figure 9. All rotation speeds: Mass and efficiency of direct and geared drive superconducting machines with different rotation speeds n_{EM}. The faded data symbols represent about five percent of all machines which have been computed. The bold colored symbols show machines that are pareto-optimal with respect to mass and efficiency. The pareto curve is extracted from all computed machines. The direct-drive $n_{EM} = 3500$ min^{-1} (blue dots) achieves the highest efficiency, however also the highest minimum mass. In contrast, the machines with $n_{EM} = 15000$ min^{-1} achieve the lowest minimum mass of 167 kg only, but are also the least efficient machines.

meaning that for a particular mass the machine can not achieve any superior efficiency and vice versa.

In figure 8 the influence of the number of pole pairs that directly translates into the electric frequency f_{el} on the mass and the efficiency of the machines with $n = 3500$ min^{-1} is presented. Whereas the loss increases almost linearly with the number of pole pairs, mirroring the frequency-dependent AC loss of the MgB_2 coils in the stator and the iron yoke, the machines with higher pole pairs are the lightest. The latter behavior is linked to the required thickness of the yoke which scales inverse with the number of pole pairs $\propto 1/p$. Furthermore, these results already indicate that machines of higher mechanical rotation speeds, featuring larger electric frequencies for the same number of pole pairs p, an enhanced cooling effort is expected.

In figure 9 the pareto-optimal machines for all mechanical rotation speeds are depicted. The curves show that the higher the rotation speed of the machine the lower the possible achievable mass is, but reducing the achievable efficiencies that are the highest for $n_{EM,EPU} = 3500$ min^{-1}. The lightest machine at $n_{EM,EPU} = 15000$ min^{-1} weights only 167 kg but produces $Q_{stator} = 7800$ W stator coil losses and $Q_{yoke,iron} = 8250$ W losses in the iron yoke of the stator when operated in the design point. The choice of a particular machine and rotation speed will depend on the other components and the mass of the required cooling systems that will be elaborated in the next sections.

4.2. Gearbox

In figure 10 the combined mass and efficiency of the two superconducting machines that share the same shaft and the respective gearbox to transmit the rotation speed of the machine and the fan are shown. Due to the mass of the gearboxes, the advantages machines with high rotation speed showed (compare to figure 9) are removed almost completely. Systems with $n_{EM} = (5000, 7500)$ min^{-1} are even heavier than the direct-drive solution, not shown here for clarity of the figure. Firstly, this is caused by the higher mass of these superconducting machines when compared to $n_{EM} = (10\,000, 15\,000)$ min^{-1} and secondly by the higher mass of gearboxes with small transmission ratios. It should be noted that the mass of the lubrication oil and the heat exchanger to cool the oil of the gearbox are not included in the results of figure 10. For gearboxes with efficiencies of about 99.5% cooled with lubrication oil, we estimate that the oil has almost the same mass as the gearbox itself. Moreover, using optimistic mass-to-power densities for oil-air heat exchangers of about 0.7 kg kW^{-1} [37] , another 70 kg would add to the geared drive solutions.

4.3. Cryogenic power electronics

In figure 11 the results of a 10.5 MW inverter for different topologies are shown. To allow better comparison machines with a power factor of $\cos\phi = 0.90$ were assumed to be connected to these inverters. The lowest mass can be achieved for the 2L-topology, whereas the highest efficiencies are

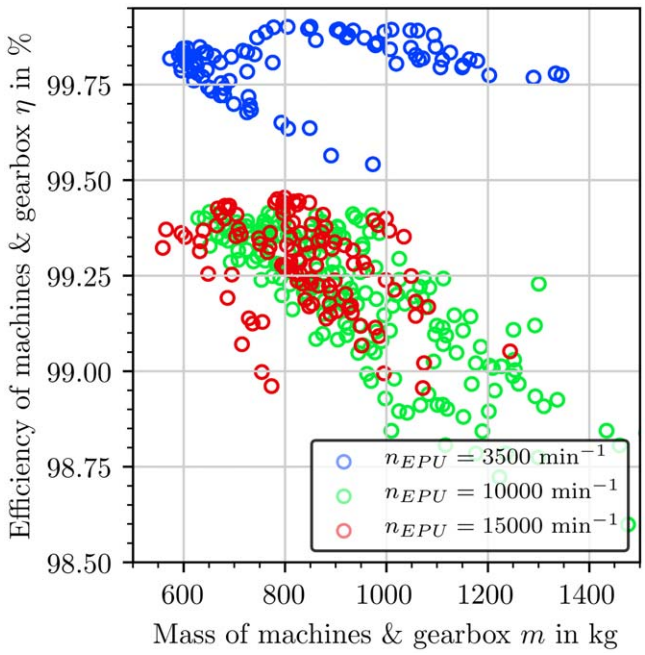

Figure 10. Influence of gearbox: Mass and efficiency of two two superconducting machines in row and the gearbox with the respective transmission ratio between the fan n_{fan} and the superconducting machines n_{EM}.

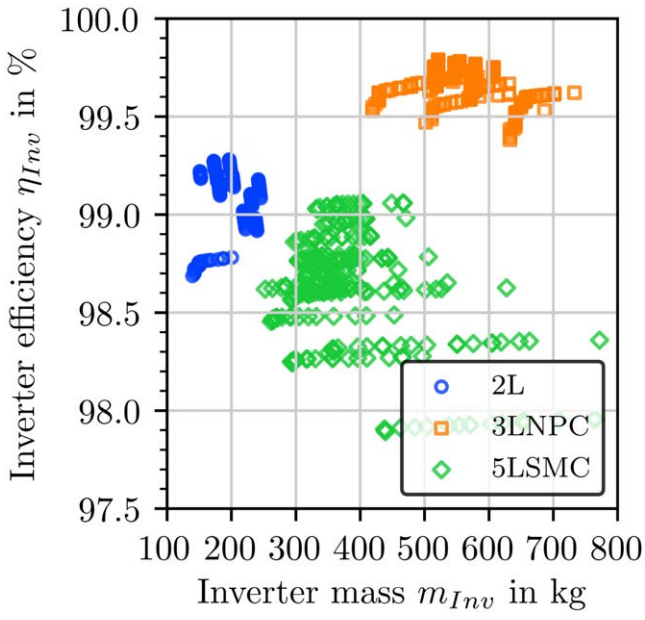

Figure 11. Influence of the inverter topology: The 2L topologies (blue circles) enable the lightest designs by achieving efficiencies of up to 99.5%. The 3LNPC topology (orange cubes) is more than a factor of two heavier, but the losses are about a factor of three smaller, enabling efficiencies of up to 99.75%. The 5L SMC architectures (green diamonds) are mostly lighter than the 3LNPC and heavier than the 2L, but show the worst efficiencies among the three architectures.

reached with the 3LNPC topology, however, linked with nearly twice the mass per inverter.

To illustrate the influence of the DC voltage level, the mass of the 3LNPC topology is shown for different voltages

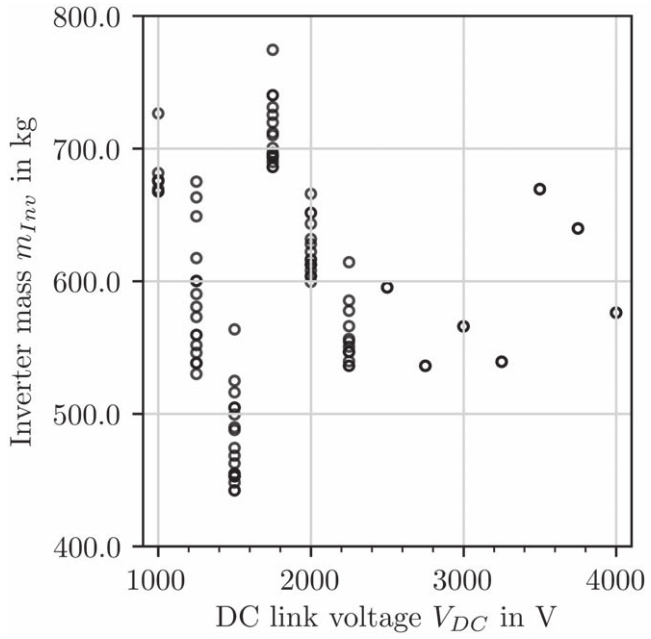

Figure 12. 3LNPC inverter, influence of the DC voltage level: the inverters at 1500 V are the lightest, whereas inverters at 1750 V are significantly more heavy. This non-continuous behavior is linked to 3-level topology using half bridges and the maximum module operating voltage of 850 V.

in figure 12. Even though there is a band of inverters for each DC voltage level (they belong to different electrical frequencies), it is very prominent that the mass of the inverters is the smallest for $V_{DC} = 1500$ V sharply increasing for $V_{DC} = 1750$ V. For even higher voltages the mass of the inverter decreases before significantly increasing again at $V_{DC} = 3500$ V. Both effects are linked to the utilization of the blocking voltage of the modules. In the 3LNPC- inverter topology half-bridges are used. Therefore, for multiples of twice the operating blocking voltage V_{op}, here $V_{op} = a_{cosmic} \cdot V_{block} = 0.5 \cdot 1700$ V, the utilization of the modules is optimal, whereas slightly larger voltages require a second module connected in series. This effect underlines the importance of representing the components in detailed models instead of using simple scaling equations.

The inverter has to deliver the electric frequencies which fit the superconducting machines. Different combinations of the machines' mechanical rotation speed and the pole pair number lead to a non-equidistant distribution of realizable electric frequencies. The electric frequency has a direct influence on the switching losses and the choice of EMI filters. For the 3LNPC topology, the losses of the inverters for different electric frequencies and voltages are shown in figure 13. For each voltage level, the losses increase almost linearly with increasing electric frequency without showing an optimum.

4.4. HTS DC transmission

Two examples of the voltage dependence of the specific mass per meter are shown in figure 14. The fast decrease of the

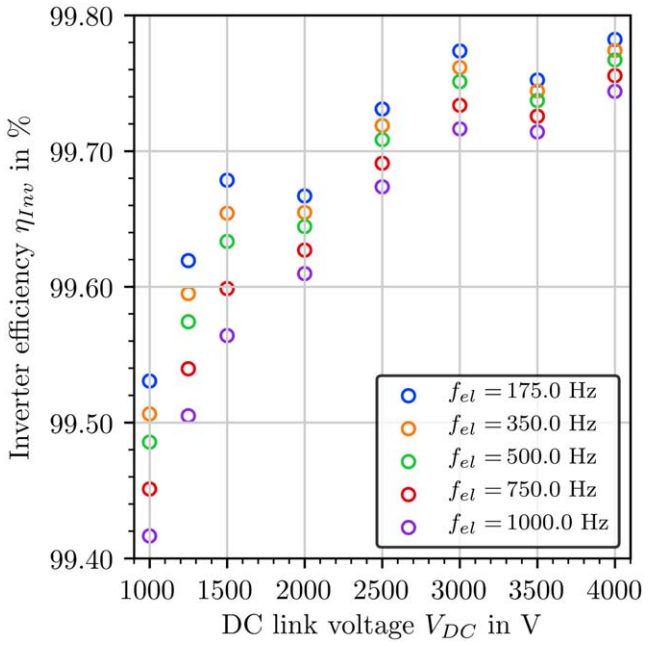

Figure 13. Efficiency 3LNPC inverter: Dependency of the inverter efficiency on the level of the DC voltage for different electric frequencies. Similar to the behavior of the mass, also the efficiencies tend to improve for higher voltage levels, whereas voltages just above twice the operating blocking voltage of the module break this trend.

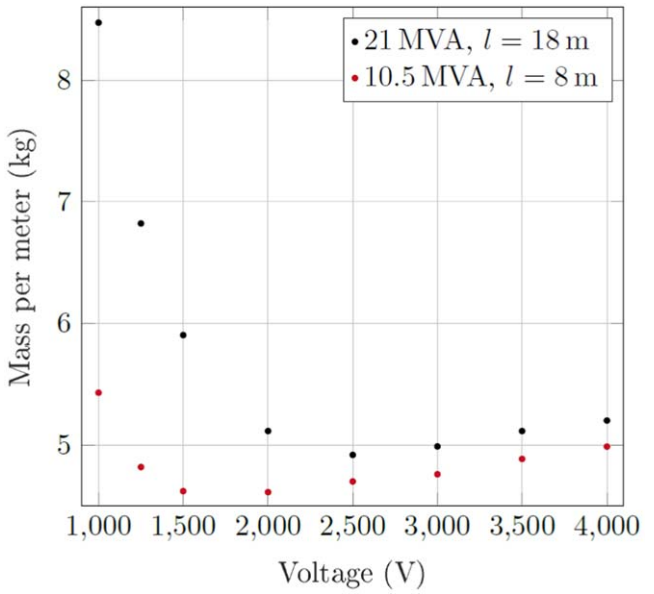

Figure 14. Voltage dependence: Specific mass per meter for different voltage levels for two different transmission lines with 20 MVA (generation to power distribution center) and 10 MVA (power distribution center to EPUs). Both power distributions show a minimal specific mass (10.5 MVA: (1500V|7000A), 21.0 MVA: (2500V|8400A)). For small voltages the mass of the current leads contribute significantly and the large forces between the poles require a pole to pole distances that lead to larger diameters of the cryostats. For higher voltage levels, the specific masses slightly increases. This is related to the increasing pole to pole and pole to wall distances due to insulation requirements.

mass in between 1000 and 2500 V can be explained by the smaller mass of the current leads and the smaller distance between the poles due to smaller currents. In contrast, for even higher voltage levels, the criteria linked to insulation become dominant, thus scaling the distance between the two poles and themself and the poles and the cryowall. Therefore, the mass of the transmission system slightly increases.

4.5. Electric propulsion unit

The dependency of the system KPIs as mass and efficiency on the DC voltage level and the electric frequencies of the propulsion- and generation-unit are investigated. Due to the high complexity of the total drive train system, the influence of the global variation parameters and the choice of a direct drive or geared drive system is first presented for the electric propulsion unit without taking into account the cooling system (section 4.5). In a second step, the complete drive train is presented. By including the required masses of the liquid hydrogen tank to cool the losses during the mission (see figure 1(b)), a fair assessment of mass and efficiency of the drive train is achieved. Therefore, the performance of the electric components during the different phases of the mission have been computed.

To compute the mass and the efficiency of the electric propulsion unit, the components which share the same electrical (V_{DC}, $f_{el,EPU}$) and mechanical parameters (rotation speed of the superconducting machines n_{EM}) are combined. The mass of a EPU contains the mass of the two machines, the DC/AC inverters, the power distribution and the potentially required gearbox between the machine and the fan. The efficiency of the EPU is calculated as the product of the in-series components. The mass and efficiency of a single EPU without the mass for cooling categorized by the inverter topology is shown in figure 15. The results are clustered in two distinct areas which are linked to the different inverter topologies (2L and 3LNPC). As on the component level (figure 11) subsystems using a 2L inverter are lightest whereas subsystems with 3LNPC inverters are the most efficient, but heavier. However, when adding the required amount of liquid hydrogen and its storage tank for the mission of the aircraft, lower efficiencies experience a higher penalty mass, clearly favouring the 3LNPC technology on the subsystem level, displayed in figure 16.

When grouping the same set of data by the mechanical rotation speed of the superconducting machine (figure 17, the direct drive, and the geared drive solution can be compared (see figure 17)). Whereas for the machines alone higher mechanical rotation speeds tend to have the lightest mass (figure 9), adding the optional gearbox, inverters, cables and cooling remove this advantage almost completely. Mostly, this is caused by the additional mass and loss the use of a gearbox to fit the rotation speeds of the machines and the fan. Prominently, the efficiency of the direct drives is higher compared to the high-rpm geared drives. This effect is linked to the higher losses of the machines (Figure 9) and the inverters (figure 13) when increasing the electric frequency. Moreover, the gearbox adds another element of finite efficiency. Therefore, one can state that the 3LNPC inverter

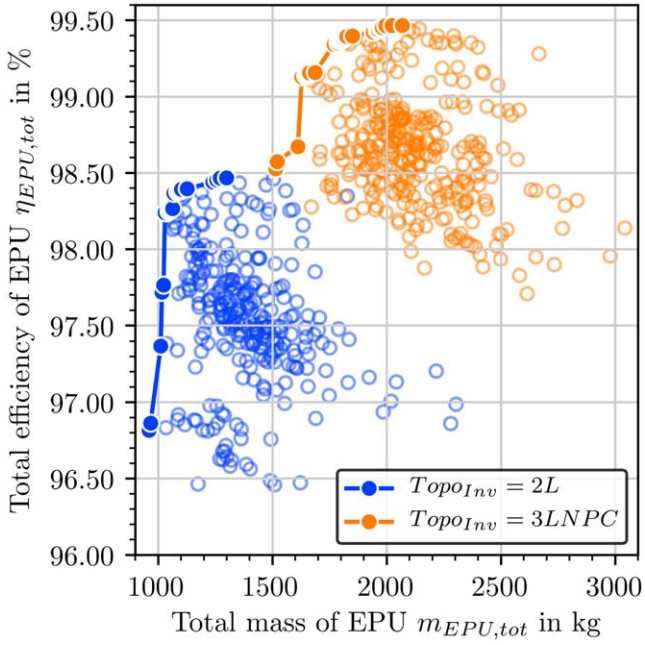

Figure 15. Mass and efficiency of a single EPU for different topologies of the inverter: EPUs with 2L topologies reach lower mass than 3LNPC technologies, whereas the efficiencies behave vice versa.

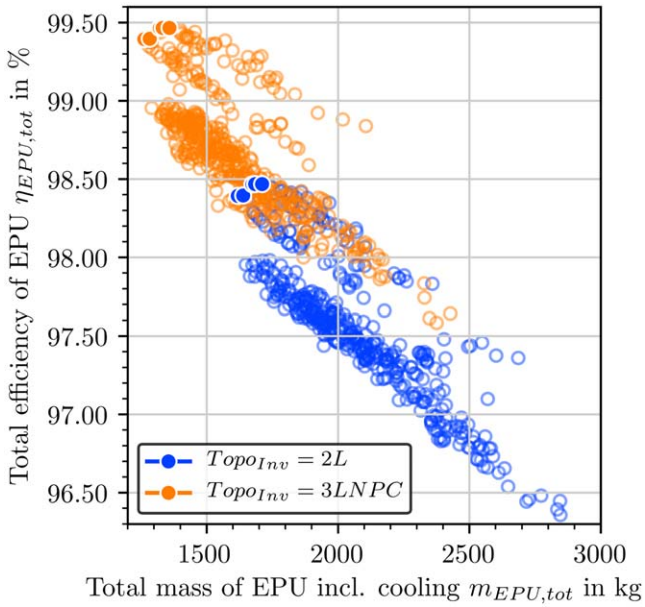

Figure 16. Mass and efficiency of a single EPU including penalty mass for cooling: When adding liquid hydrogen and its storage tanks that are required during the mission of the aircraft, the EPUs which use the 3LNPC inverter topology are favoured in mass and efficiency.

technology and the direct drive solutions are the favoured configurations for the EPU.

4.6. Total CEPS

To construct the whole drive train which is depicted in figure 2 the EPU and the generation subsystems which share

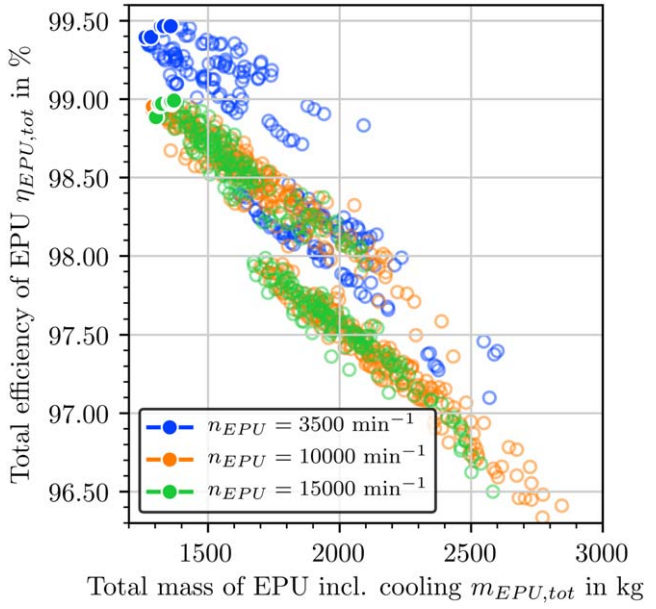

Figure 17. Direct drive versus geared drive solution: Mass and efficiency of the EPUs when pre-selecting the 3-level architecture and grouping the results by the rotation speed of the superconducting machines. The direct drive solutions are more efficient and lighter in mass compared to the geared solutions.

the same DC bus voltage have to be combined. The generation units were computed in the same way as the EPUs. Even though they are not shown here in detail, it should be noted that an electric frequency of 500 Hz and the 3LNPC inverter topology resulted in the most efficient and lightest generation units. Thus, only direct drive solutions with 3LNPC inverter topologies are considered on the system level. The only remaining variable global parameter is the DC bus voltage and the electric frequency of the EPU. Figure 18 shows the total mass and efficiency of drive trains for different system voltages between 1000 and 4000 V and two different electric frequencies of the electric propulsion unit. For each voltage level, the results accumulate in two clouds, $f_{el} = 350.0$ Hz featuring lighter masses while $f_{el} = 175.0$ Hz are more efficient. Independent of the electric frequency systems with $V_{DC} = 1000$ V are the heaviest and least efficient. At first glance, the systems become lighter and more efficient the higher the voltage level gets. However, similar as for the inverters (figures 12 and 13) voltage levels of 1500 V and 3000 V break this trend. A system with a voltage level of $V_{DC} = 1500$ V and an electric frequency $f_{el} = 350$ Hz is the lightest propulsion system with a mass of $M_{Sys} = 8355$ kg.

To understand the origin of this behavior on the system level, the lightest systems for each set of voltage and electric frequency are selected and decomposed into the masses of the components. This mass breakdown is shown in figure 19. The cabling of the HTS power distribution that already includes the required current leads has the smallest contribution to the mass of the system and does not show a strong dependence on the choice of the voltage level. Even if the size of the current lead is known to be very sensitive to the current, in this study, its absolute mass is rather small since the temperature hub is

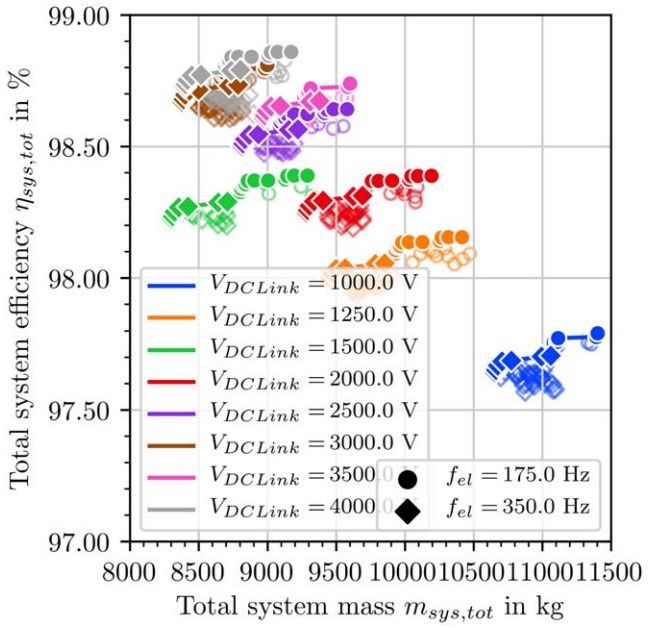

Figure 18. Total drive train: Mass and efficiency of the whole drive train in dependency of the voltage level $V_{DC,link}$ of the DC bus and the electric frequency f_{el} of the direct drive electric propulsion unit. Face colored data are pareto optimal for the respective set of voltage and electric frequency. For reasons of clarity only five percent of all other data (white faced) are illusrated.

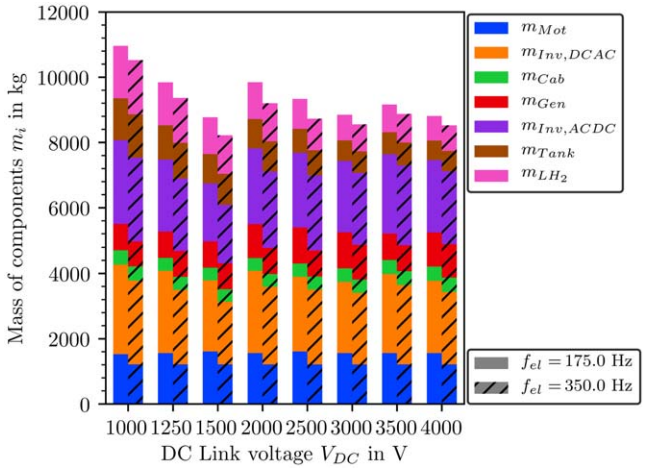

Figure 19. Total drive train: Total mass and efficiency of the whole drive train in dependency of the voltage level of the DC link V_{DC} and the electric frequency f_{el} of the EPU.

rather small. The electric machines and generators do not show a large dependency on the DC link voltage as well and have a combined mass share of about 30% of the total system mass. For all voltage levels and frequencies, the power electronics has the largest share among the system mass. Even in the case of lightest power electronics, $V_DC = 1500$ V,$f_{el} = 350$ Hz, they contribute 44% to the mass of the system. This value becomes even more decisive when accounting for the mass of the cooling system to remove the loss of the inverters that are the highest of the electric components. The mass of the inverters is the smallest for $V_{DC} = 1500$ V and $V_{DC} = 3000$ V, again linked to the voltage utilization of the modules. The only reason why systems operated at 4000 V are in a similar range of system mass, is their higher efficiencies which result in a smaller mass of the required LH_2 and its storage tanks.

Table 2. Filtered results for three different system voltages, focused on the characteristics of the electrical machines. The machines belong to the systems with the highest system efficiency and a system mass below 8500.0 kg. Even though the systems are lightest for 1500 V, the required volume of LH_2 is significantly higher.

Type	Symbol	Unit	Value	Value	Value
Global	V_{DC}	V	1500	3000	4000
	M_{Sys}	kg	8355	8432	8417
	η_{Sys}	%	98.27	98.71	98.75
	m_{equi}	kg	3900	2744	2618
	M_{eff}	kg	4455	5688	5799
EPU	f_{el}	Hz	350	350	350
	n_{EM}	min^{-1}	3500	3500	3500
	P_{EM}	MW	10.5	10.5	10.5
	d_{EM}	m	0.52	0.55	0.54
	l_{EM}	m	0.54	0.63	0.62
	m_{EM}	kg	287	304	303
	η_{EM}	%	99.90	99.92	99.92
	$B_{S,EM}$	T	1.17	0.91	0.90
	$Q_{S,EM}$	W	4378	2393	2396
	$Q_{Fe,EM}$	W	5077	5653	5680
	m_{Inv}	kg	479	545	554
	η_{Inv}	%	99.65	99.76	99.77
Gen	f_{el}	Hz	500	500	500
	P_{EM}	MW	21.0	21.0	21.0
	n_{EM}	min^{-1}	10 000	10 000	10000
	d_{EM}	m	0.37	0.36	0.37
	l_{EM}	m	1.02	1.21	1.02
	m_{EM}	kg	376	398	375
	η_{EM}	%	99.87	99.92	99.90
	$B_{S,EM}$	T	0.82	0.73	0.81
	$Q_{S,EM}$	W	2645	2062	2640
	$Q_{Fe,EM}$	W	6740	6461	6730
	m_{Inv}	kg	886	1096	1114
	η_{Inv}	%	99.63	99.74	99.76
Cool	m_{LH_2}	kg	1187	831	793
	V_{LH_2}	l	16 765	11 737	11200
	n_{Tanks}		2 × 2	2 × 2	2 × 2
	$m_{Tank,C}$	kg	n.a.	n.a.	237.0
	$l_{Tank,C}$	m	n.a.	n.a.	2.37
	$d_{Tank,C}$	m	n.a.	n.a.	1.19
	$t_{Tank,C,Al}$	mm	n.a.	n.a.	1.65

Table 2 lists the three systems that were found to be the lightest. When comparing these results to the requirements that have been listed in table 1, the maximum allowed size of the machines can be achieved and even surpassed. Furthermore, the superconducting machines in the EPU are operated with higher flux densities in the working point of the stator $B_{S,EM}$ than the superconducting generators. This is linked with the higher electric frequency f_{el} in the generation unit that increases AC losses and therefore lowers the achievable

current density in the stator. This effect has been investigated extensively already in [19].

The lower overall system efficiency at 1500 V leads to the significantly higher amount of required hydrogen to cool the components during the mission compared to higher voltage levels. When assuming that the hydrogen m_{LH_2} can be used further for combustion, an energy-equivalent amount of kerosene m_{equi} can be subtracted from the system mass M_{Sys}, resulting in an effective mass of the system M_{eff}. At first glance, the case of 1500 V seems to be preferable. However, the required volume V_{LH_2} to store the hydrogen exceeds the requirement in 1 of the maximum accessible space by far. Moreover, due to the strongly reduced installation space that was assumed to be constrained by the volumes of the original kerosene fuselage tanks, even the case of 3000 V does not fit to the given requirements. No storage tank could be designed that fulfills the geometrical and thermal requirements, even though the total required amount of liquid hydrogen is only about 40 kg higher than in the selected case of 4000 V. This underlines that the design of such propulsion system would require strong iterative exchange with the design of the aircraft itself.

5. Summary and conclusion

By using analytical models for each component of a turboelectric drive train that features superconductivity and is cryogenic-cooled with liquid hydrogen, a study of a re-equipped mid-range passenger aircraft was performed. The models use the characteristics of superconductors, power electronics equipment and materials that are either currently under development or commercially available.

Direct and geared electric propulsion systems that drive a fan with the characteristics of an actual turbofan engine with $n_{fan} = 3500\,\mathrm{min}^{-1}$ are compared. Even though superconducting machines with higher rotation speeds are advantageous in mass, additional gearboxes and the hydrogen cooling system cause the more efficient direct drive electric propulsion units with $n_{EM,EPU} = 3500\,\mathrm{min}^{-1}$ to be the preferable solution on a system level. However, it should be noted that in a coupled optimisation of a fan- which trends to be more efficient for lower rotation speed and larger diameter [13]- and the electric propulsion unit might change this result.

Moreover, the dependency of the total system mass of the direct drive solutions on the choice of the DC voltage link was evaluated. It was found that low voltages of 1000 V are not a sufficient choice. Due to large required currents, the mass of the power distribution increased and the efficiency of the power electronics decreased compared to higher voltage levels. However, even if the best efficiencies and lowest masses tend to occur at the higher voltages of the investigated range, no general statement can be extracted. Prominently, the voltage level of $V_{DC} = 1500$ V and electric frequencies of $f_{el,EPU} = 350.0$ Hz results in the lowest possible system mass of $M_{Sys} = 8355$ kg. This effect is strongly linked to the 3LNPC inverters that reach their lowest mass at $V_{DC} = 1500$ V since the voltage utilization of the Si IGBT switching module is close to their optimum. This effect underlines the importance to use detailed models to describe the components instead of simple scaling equations.

In general, the largest share of the system mass is linked to the inverters in the system. Firstly, due to the mass of inverters themselves and secondly due to their losses that drive the mass of the liquid hydrogen cooling system. Therefore, further research on low loss and radiation-hard power electronics that can be operated in the cryogenic range will have a large influence on the overall system performance [38]. Moreover, a comprehensive examination of the thermal management of the whole system, i.e. optimisation of the component's operational temperature, remains a future task. Especially a more detailed assessment of the gearbox cooling process as well as temporal evolution of the hydrogen tanks during operation remain a challenge. The total effective mass of the systems M_{eff} showcases the challenge hybrid-electric propulsion of mid-range passenger aircraft will face. To make such systems advantageous, the overall system efficiency including the turboshaft machines and the fans would need to compensate for the additional payload. But, breaking up the generation of power and thrust opens the design space for novel aircraft configurations [3, 39].

Acknowledgments

The authors acknowledge the financial support by the Federal Ministry for Economic Affairs and Energy of Germany in the framework of LuFoV-2 (project number 20Y1516C). We thank Bernhard Holzapfel, Philipp Weber, Alexander Zakrzewski, Mabroor Ahmed, Lars Kuehn, Joern Grundmann, Marijn P Oomen and Tabea Arndt for helpful discussions.

ORCID iDs

Martin Boll https://orcid.org/0000-0002-9778-4280

References

[1] International Air Transport Association *et al* Iatatechnology roadmap. June, 2013
[2] Darecki M *et al* 2011 Flightpath 2050 Europe's vision for aviation *Off. Eur*
[3] Felder J, Kim H and Brown G 2009 Turboelectric distributed propulsion engine cycle analysis for hybrid-wing-body aircraft *47th AIAA aerospace sciences meeting including the new horizons forum and aerospace exposition* p 1132
[4] DelRosario R 2014 A future with hybrid electric propulsionsystems: A nasa perspective
[5] Schulz E 2018 Global networks, global citizens. global market forecast 2018-2037. Airbus (Ed.). Blagnac Cedex, France,2018
[6] Berg F, Palmer J, Miller P and Dodds G 2017 Hts system and component targets for a distributed aircraft propulsion system *IEEE Trans. Appl. Supercond.* **27** 1–7

[7] Wheeler P 2016 Technology for the more and all electric aircraft of the future *2016 IEEE Int. Conf. on Automatica (ICA-ACCA)* (Piscataway, NJ: IEEE) pp 1–5

[8] Hornung M, Isikveren A T, Cole M and Sizmann A 2013 Celiner-case study for emobility in air transportation *2013 Aviation Technology, Integration, and Operations Conf.* p 4302

[9] Brewer G D 2017 *Hydrogen Aircraft Technology* (Boca Raton, FL: CRC Press)

[10] Corchero G and Montanes J L 2005 An approach to the use of hydrogen for commercial aircraft engines *Proc. Inst. Mech. Eng* G **219** 35–44

[11] Westenberger A 2016 Hydrogen and fuel cells: mobile application in aviation *Hydrogen and Fuel Cell* (Berlin: Springer) pp 107–25

[12] 2019 *Aircraft Characteristics: Airport and Maintenance Planning* AIRBUS S.A.S. (https://www.airbus.com/content/dam/corporate-topics/publications/backgrounders/techdata/aircraft_characteristics/Airbus-Commercial-Aircraft-AC-A321.pdf)

[13] 2019 *Geared turbofan commercial engines* Pratt & Whitney http://newsroom.pw.utc.com/download/PW1100G-JM.pdf

[14] Annushkin Y M and Maslov G F 1985 Efficiency of combustion of hydrogen-kerosene fuel in a straight duct *Combust. Explosion Shock Waves* **21** 297–8

[15] Easa C 2009 *Certification Specifications for Large Aeroplanes* CS25 (https://www.easa.europa.eu/sites/default/files/dfu/CS-25_Amdt%203_19.09.07_Consolidated%20version.pdf)

[16] Filipenko M, Kuehn L, Haese K, Moldenhauer S, Grundmann J, Lessmann M, Boehm M, Frank M and van Hasselt P 2020 Concept design of a high power superconducting generator for future hybrid-electric aircraft *Supercond. Sci. Technol.* (https://doi.org/10.1088/1361-6668/ab695a)

[17] Greatrix D R 2012 Turboprop and turboshaft engines *Powered Flight* (Berlin: Springer) pp 269–89

[18] Sumption M D 2019 Ac loss of superconducting materials-refined loss estimates for very high density motors and generators for hybrid-electric aircraft: Mgb2 wires, coated conductor tapes and wires *AIAA Propulsion and Energy 2019 Forum* p 4495

[19] Corduan M, Boll M, Bause R, Oomen M, Filipenko M and Noe M 2020 Topology comparison of superconducting ac machines for hybrid-electric aircraft *IEEE Trans. Appl. Supercond.* **30** 5200810

[20] Kisssoft A G 2019 Kisssys (https://www.kisssoft.ch/english/products/kisssys.php)

[21] Mizutani H, Isikawa Y and Townsend D P 1989 *Effects of Lubrication on the Performance of High Speed Spur Gears* N-89-22919 National Aeronautics and Space Administration, Cleveland OH

[22] Graber L, Saeedifard M, Mauger M J, Yang Q, Park C, Niebur T, Pamidi S V and Steinhoff S 2017 Cryogenic power electronics at megawatt-scale using a new type of press-pack igbt *IOP Conf. Series: Materials Science and Engineering* vol 279 (Bristol: IOP Publishing) p 012011

[23] Rajashekara K and Akin B 2013 Cryogenic power conversion systems: the next step in the evolution of power electronics technology *IEEE Electrification Mag.* **1** 64–73

[24] Caiafa A, Wang X, Hudgins J L, Santi E and Palmer P R 2003 Cryogenic study and modeling of igbts *IEEE 34th Annual Conf. on Power Electronics Specialist, 2003. PESC'03* vol 4 (Piscataway, NJ: IEEE) pp 1897–903

[25] Krug D 2016 Vergleichende untersuchungen vonmehrpunkt-schaltungstopologien mit zentralem gleichspannung-szwischenkreisfür mittelspannungsanwendungen (https://d-nb.info/1123931275/34)

[26] Yang S 2005 Cryogenic characteristics of IGBTs *PhD Thesis* University of Birmingham

[27] Akturk A, Wilkins R, McGarrity J and Gersey B 2016 Single event effects in si and sic power mosfets due to terrestrial neutrons *IEEE Trans. Nucl. Sci.* **64** 529–35

[28] Teyssandier F and Prêle D 2010 Commercially available capacitors at cryogenic temperatures *Ninth Int. Workshop on Low Temperature Electronics-WOLTE9*

[29] Wolf M J *et al* 2017 HTS CroCo: a stacked HTS conductor optimized for high currents and long-length production *IEEE Trans. Appl. Supercond.* **26** 19–24

[30] 2018 *Thev Pro-Line TPL 4100* Theva (https://www.theva.de/wp-content/uploads/2018/08/THEVA-TPL4100-datasheet-08-2018-1.pdf)

[31] Stephan P *et al* 2019 *VDI-Waermeatlas* (Berlin: Springer)

[32] Xu Z and Grilli F 2015 Modelling ac ripple currents in hts coated conductors *Supercond. Sci. Technol.* **28** 104002

[33] Winnefeld C, Kadyk T, Bensmann B, Krewer U and Hanke-Rauschenbach R 2018 Modelling and designing cryogenic hydrogen tanks for future aircraft applications *Energies* **11** 105

[34] Sekaran P R, Gohardani A S, Doulgeris G and Singh R 2014 Liquid hydrogen tank considerations for turboelectric distributed propulsion *Aircraft Eng. Aerosp. Technol.* **86** 67–75

[35] Stroman R O, Schuette M W, Swider-Lyons K, Rodgers J A and Edwards D J 2014 Liquid hydrogen fuel system design and demonstration in a small long endurance air vehicle *Int. J. Hydrogen Energy* **39** 11279–90

[36] Millis M G, Tornabene R T, Jurns J M, Guynn M D, Tomsik T M and VanOverbeke T J 2009 *Hydrogen Fuel System Design Trades for High-Altitude Long-Endurance Remotely-Operated Aircraft* NASA (https://ntrs.nasa.gov/archive/nasa/casi.ntrs.nasa.gov/20090013674.pdf)

[37] Vratny P C 2019 Conceptual design methods of electric power architectures for hybrid energy aircraft *PhD Thesis* Technische Universität München

[38] Gonzalez M C, Kohlman L W and Trunek A J 2018 *Cryogenic Parametric Characterization of Gallium Nitride Switches* NASA (https://ntrs.nasa.gov/archive/nasa/casi.ntrs.nasa.gov/20180005716.pdf)

[39] Seitz A *et al* 2018 Concept validation study for fuselage wake-filling propulsion integration *31st Congress of the Int. Council Aeronautical Sciences* pp 9–14